Review of Scientific Instruments

High sensitivity detection of nanoparticles permeation through polymer membranes: A physico-chemical and nuclear imaging measurement approach

Cite as: Rev. Sci. Instrum. **93**, 123703 (2022); https://doi.org/10.1063/5.0087704
Submitted: 08 February 2022 • Accepted: 06 November 2022 • Published Online: 06 December 2022

Mahmoud Mohamed Omar, Mariia Kiseleva, Myriam Laprise-Pelletier, et al.

Review of Scientific Instruments ARTICLE scitation.org/journal/rsi

High sensitivity detection of nanoparticles permeation through polymer membranes: A physico-chemical and nuclear imaging measurement approach

Cite as: Rev. Sci. Instrum. 93, 123703 (2022); doi: 10.1063/5.0087704
Submitted: 8 February 2022 • Accepted: 6 November 2022 •
Published Online: 6 December 2022

Mahmoud Mohamed Omar,[1,2] Mariia Kiseleva,[1,2] Myriam Laprise-Pelletier,[1,2] Amelie Auge,[1,2] Ludovic Tuduri,[3,a)] and Marc-André Fortin[1,2,b)]

AFFILIATIONS

[1] Département de Génie des Mines, de la Métallurgie et des Matériaux, Centre de Recherche sur les Matériaux Avancés (CERMA), Université Laval, Québec G1V 0A6, Canada
[2] Axe Médecine Régénératrice, Centre Hospitalier Universitaire (CHU) de Québec, 2705, Blvd. Laurier (T1-61a), Québec G1V 4G2, Canada
[3] Centre National de la Recherche Scientifique (CNRS), Unité Mixte de Recherche 5805, Environnements et Paléoenvironnements Océaniques et Continentaux (EPOC), Équipe Physico et Toxico Chimie de l'environnement, Université de Bordeaux, Talence, France

[a)] Formerly at: Institut de Recherche Robert-Sauvé en Santé et Sécurité du Travail, Montréal, Québec H3A 3C2, Canada.
[b)] **Author to whom correspondence should be addressed:** marc-andre.fortin@gmn.ulaval.ca

ABSTRACT

Diffusion cells are devices made of donor and acceptor compartments (DC and AC), separated by a membrane. They are widely used in pharmaceutical, cosmetic, toxicology, and protective equipment tests (e.g., gloves) to measure the kinetics of permeants (molecules and nanoparticles) across biological membranes as the skin. However, rarely is the concentration of permeants in the AC measured in continuous or in real-time, and this limitation leads to significant discrepancies in the calculations of kinetic parameters that define the permeation mechanisms. In this study, a diffusion cell compatible with positron emission tomography was used to measure the permeation kinetics of nanoparticles across glove membranes. The technology allows for the measurement of nanoparticle concentration in real-time in the two compartments (DC and AC) and at a detection sensitivity several orders of magnitude higher compared with conventional spectroscopies, thus allowing a much more precise extraction of kinetic parameters. Ultra-small (<10 nm) gold nanoparticles were used as a model nanoparticle contaminant. They were radiolabeled, and their diffusion kinetics was measured in continuous through latex and nitrile polymer membranes. Permeation profiles were recorded at sub-nanomolar sensitivity and in real-time, thus allowing the high precision extraction of kinetic permeation parameters. The technology, methodology, and data extraction process developed in this work could be applied to measure in real-time the kinetics of diffusion of a whole range of potentially toxic molecules and nanoparticles across polymer membranes, including glove membranes.

NOMENCLATURE

AC	acceptor compartment
ATR-FTIR	attenuated total reflectance Fourier transform infrared spectroscopy
DC	donor compartment
DFO	deferoxamine B mesylate salt
EDS	energy-dispersive x-ray spectroscopy
FDC	Franz diffusion cell
ICP-AES	inductively coupled plasma atomic emission spectroscopy
ICP-MS	inductively coupled plasma mass spectrometry
LOD	limit of detection
LOQ	limit of quantification

MP-AES	microwave-plasma absorption emission spectroscopy
NPs	nanoparticles
PPE	personal protective equipment
PET	positron emission tomography
ROI	region of interest
SEM	scanning electron microscopy
USNP	ultra-small nanoparticles (<10 nm diameter)
UV–vis	ultraviolet–visible spectroscopy

I. INTRODUCTION

Nanotechnologies are now integrated into a large number of consumer goods, cosmetics, and healthcare products. By the year 2019 and for the medical sector only, more than 27 nanoparticles-based medicines had been approved by either the Food and Drug Administration (FDA) or the European Medicines Agency (EMA). More than 50 new products are currently in clinical trials under the roadmaps of the FDA and the EMA.[1]

The fabrication of nanoparticles (NPs) involves exposure of workers to such substances. While the final products can be safe, workers involved at each step of the manufacturing process are exposed to different amounts, doses, and concentrations of NPs. Because NPs are complex materials available in an infinity of different sizes, compositions, and surface chemistries, certain can be manipulated without personal protective equipment (PPE), while others are suspected to cause injuries to the skin, the eyes, the lungs, etc. In general, the principle of precaution applies to limit the occupational exposure of workers to NPs. Gloves must be worn by the workers involved in the fabrication of NPs.

The skin is the largest organ of the body. It acts as a barrier that separates the internal organs from the surrounding environment. In work environments, the skin comes in contact with several products that might cause dermatitis. In fact, skin-related occupational contact dermatitis is among the most frequent work-related condition. It is estimated that each year, a total of 1×10^9 dollars are directed toward treating this condition in the USA only.[2] The problematics of occupational dermal exposure to NPs and nano-enabled products were described in two recent papers by Brouwer *et al.*[3,4] Gloves are possibly the most used PPE for the reduction of occupational contact dermatitis.[5] Several standardizing organizations such as the American Society for Testing and Materials (ASTM), the International Standard Organization (ISO), and the Committee for European Normalization (CEN) have developed test methods to characterize and quantify the resistance of polymeric glove membranes against solvents, potentially toxic molecules, and NPs including viruses.[6–11]

Permeation tests are the cornerstone of glove testing, and they usually involve the use of diffusion cells.[7,9–11] In fact, diffusion cells have emerged from the field of pharmacology; they are also widely used in cosmetics testing and for membrane permeation science, in general. The device is made up of two compartments: one donor compartment (DC) and one acceptor compartment (AC), separated by the tested membrane.[12] The substance to be tested for its diffusion properties (i.e., the "permeant") is added to the DC and allowed to diffuse through the membrane and into the AC from which it can be sampled and measured. Among the measurement technologies used to measure the permeant concentration, figure chromatography, spectroscopy, and spectrometric technologies mainly performed off-line and as batch tests. Permeation profiles are thus revealed at various levels of accuracy and sensitivity.[12] However, with a spectrometric technology such as ICP-MS, possibly the elemental analysis allowing the highest sensitivity for the detection of metallic elements in liquids, gold NPs cannot be detected at concentrations lower than 5 nmol.[13,14] This limitation in sensitivity, coupled with the difficulty to adapt such technologies to on-line and continuous measurements, is a limit to the accurate calculation of kinetic permeation parameters that could allow for more efficient comparisons of the protective efficiency of polymeric membranes used as PPE.

Over the last decades, several standards have been developed to guide the measurement and selection of gloves membranes used as PPE and particularly against chemical contaminants including NPs.[15–18] NPs are increasingly used in consumer care products, in cosmetics, and in medicine for drug delivery, cancer therapy, biomedical imaging, etc.[19–21] However, only a handful of studies have been reported until now describing their interactions with polymer membranes.[22–24] One of the main reasons is the lack of measurement techniques adapted to the measurement of NP permeation kinetics at high sensitivity and in real-time. Occupational hygiene services and worker's associations are still waiting for more precise NP permeation measurement data, which would allow them to adopt science-based recommendations for the manipulation of NPs in laboratories, factories, and in clinical environments.[25]

In fact, many governmental organizations acknowledge the lack of current data on the effectiveness of protective gloves against the permeation of NPs.[26–29] Advanced permeation tests allowing the extraction of the diffusion parameters for direct comparison between membranes are necessary at this step, in particular in the case of permeants containing highly toxic substances or in cases where it is absolutely essential to measure the kinetic parameters of permeant diffusion across the membranes. This is the case for the standard tests of polymer membranes used as barriers to contaminants (e.g., gloves).

Franz diffusion cells (FDC) are increasingly used in the cosmetic, personal care, and pharmaceutical industries to measure the permeation kinetics of contaminants across biological and synthetic membranes (skin simulation, quality control assessment of topical product application, etc.). Synthetic polymer membranes are also widely used in the separation industry for filtration technologies (e.g., ultrafiltration, reverse osmosis, ion exchange, and micro and ultrafiltration membranes). Therefore, the development of high sensitivity real-time detection technologies to monitor the passage of NPs and other contaminants across synthetic membranes could have a strong impact on a broad range of industrial, health, and consumer care applications.

The present study reports on the use of a diffusion cell adapted to nuclear imaging. Nuclear imaging such as positron emission tomography (PET) allows to detect photons produced by radioisotopes at a sensitivity that is much higher than that of the vast majority of measurement technologies that are usually coupled to diffusion cells. In fact, a first iteration of a diffusion cell technology adapted to PET, specifically developed for skin permeation experiments, was recently reported in the literature.[30] However, that diffusion cell was oriented toward the measurement of topical formulations of NPs on biological membranes with the acceptor compartment (AC) completely open to the exterior and thus not appropriate for the comprehensive measurement of NP permeation kinetics across polymer membranes exposed to circulating fluids on

their both sides. This is a much more relevant and standard configuration for permeation measurements across membranes immersed in fluids (for example, ASTM F739 Standard "*Standard Test Method for Permeation of Liquids and Gases Through Protective Clothing Materials Under Conditions of Continuous Contact*"). In this present study, the authors have developed a diffusion cell technology adapted to nuclear imaging (PET, in particular), which allows for the measurement of kinetic parameters of NP permeation across polymer membranes in a configuration that is much closer to that widely used in a majority of standards in the field of diffusion cell measurements. In the present study, a new and optimized diffusion cell was tested with glove membranes that are widely used in the healthcare field as well as in laboratories involved in the development of biomedical NPs (latex, nitrile).

Ultra-small nanoparticles (USNPs) with a core size between 1 and 10 nm have gained much interest in nanomedicine because these products can be more efficiently eliminated by the kidneys compared with higher-sized NPs. Therefore, there is a trend toward an increased production of USNPs in the biomedical sector, which however comes with concerns related to their skin penetration, potentially leading to a surge of dermatitis cases in the worker population.[31–35] Therefore, USNPs were selected in the present study because they would allow us to address this potential issue in the field of occupational exposure.

In this study, ultra-small gold nanoparticles (US-AuNPs) were radiolabeled with a positron emitter of a half-life matching the time scale of diffusion studies (12–48 h). Then, the permeation of US-AuNPs in latex and nitrile membranes was measured by using a diffusion cell adapted to a PET measurement system. The selected membranes were representative of the PPE (gloves) validated by the health protection authorities for biomedical and medical workers manipulating NPs. The PET profiles acquired in the DC, in the AC, and in the membrane allow for the extraction of parameters describing the kinetics of NPs across gloves.

II. MATERIALS AND METHODS

A. Materials

Gold (III) chloride trihydrate ($HAuCl_4 \cdot 3H_2O$), sodium borohydride ($NaBH_4$), deferoxamine B mesylate salt (DFO), and dimethyl sulfoxide (DMSO) were purchased from Sigma-Aldrich (Canada); isopropanol, hydroxyethyl piperazineethanesulfonic acid (HEPES) buffer, and sodium carbonate (Na_2CO_3) were purchased from Fisher Scientific (Canada); acetonitrile was purchased from VWR (Canada); nitric acid and hydrochloric acid were purchased from Anachemia (Canada); pre-wetted regenerated cellulose dialysis tubes (MWCO, 25 kDa) were purchased from Spectra/Por® 6 (USA); hydrogen peroxide solution was purchased from Fluka Analytical (Canada); bi-functionalized polyethylene glycol HS-PEG-NHS (MW,1000 Da) was purchased from Biochempeg (USA); silicon substrates (one side polished) were purchased from Cemat Silicon S.A (Denmark). Carbon-coated copper grids were purchased from Canemco-Marivac (Canada); ^{89}Zr oxalate was purchased from PerkinElmer (USA); disodium salt of ethylenediaminetetraacetic acid (EDTA) and silica gel thin-layer chromatography plates (TLC silica gel 60 F_{254}) were purchased from Millipore (Canada); phosphate buffer saline (PBS, pH 7.4) was purchased from Gibco by Life Technologies (Canada); ultrapure water free from trace metals was purchased from Omni*Trace* Ultra (USA). In all experiments, nanopure water (Flex, PURELAB 18.2 mΩ, United Kingdom) was used unless specified.

B. Synthesis and characterizations of ultra-small gold nanoparticles (US-AuNPs)

US-AuNPs were synthesized using a procedure adapted from Brust *et al.*[36] The particles consist of a gold core functionalized with a stabilizing ligand (DFO grafted on PEG). DFO acts as a metal chelator for radiolabeling and PET imaging. The details of this synthesis are described in Sec. S1 of the supplementary material as well as in one of our recent papers.[30] The size and morphology of US-AuNPs were determined by dynamic light scattering (DLS) and transmission electron microscopy (TEM). The efficiency at which US-AuNPs were functionalized with the chelator ligand was demonstrated by Fourier transform infrared spectroscopy (FTIR) (see Sec. II G).

C. Radiolabeling of US-AuNPs

US-AuNPs were then radiolabeled by ^{89}Zr (half-life 3.3 days) for visualization in the PET scanner. A description of the radiolabeling procedures is provided in the supplementary material (Sec. S2). US-AuNPs–^{89}Zr were prepared in either 70% ethanol or PBS 1×. The concentration of Au in both solutions was measured by microwave plasma-atomic emission spectrometry (MP-AES, see Sec. II D) and found to be 40.8 ± 2.3 μM. The stability of ^{89}Zr chelation by US-AuNPs in both 70% ethanol and PBS 1× was measured for a period of at least 2 weeks (supplementary material, Sec. S3).

D. Sensitivity of analytical methods to US-AuNPs–^{89}Zr

To correlate data acquired from the PET system with values acquired from elemental analysis and from the gamma counter, several cross correlation curves were established. These results were also used to evaluate the Au limit of detection (LOD) of each one of the analysis methods: PET, gamma counter, MP-AES, and UV–visible absorption spectroscopy. The exact methodology is outlined in the supplementary material (Secs. S4 and S5).

E. Selection of the permeation media

In clinical and biomedical laboratory practice and before handling procedures, polymer gloves are either sterilized by 70% alcoholic solution during manipulation or washed with an aqueous solution such as saline or PBS. This treatment can induce a certain degradation of the polymer membrane. Therefore, to reproduce these conditions, the chelation stability of DFO-^{89}Zr was challenged in 70% ethanol as well as in PBS 1× (supplementary material, Sec. S3). These solutions were also used to suspend the particles dispensed in the DC and in the AC.

F. Selection and preparation of glove membranes

Latex and nitrile gloves widely used in the clinics and in biomedical nanotechnology laboratories were selected as polymers membranes for this study. All of them comply with at least one of the different standards applied to glove manufacturers in North America (see Table I). Three (3) types of nitrile membranes were chosen from commercial brands. PrimaTouch® complies with the ISO 11193-1 standard, which regulates physical parameters (dimensions,

TABLE I. List of glove membranes used for the permeation measurements.

Material	Brand	Name in this study	Reported thickness, palm (μm)[a]	Measured thickness, palm (μm)[b]	CGSB[c]	ASTM D6319[d]	ASTM F739[e]	ASTM F1671[f]	ASTM D6978[g]
Nitrile	PrimaTouch Fit®	N1	78[37]	52.1 ± 2.6	√	√	···	···	√
	Sterling SG®	N2	70[38]	52.5 ± 3.1	···	√	√	√	···
	Aquasoft®	N3	70[39]	42.9 ± 3.0	···	···	√	√	···
					CGSB	ASTM D3578[h]	EN 420:2003[i]	FDA21[j]	FDA 510(k)[k]
Latex	Microflex Evolution One®	L1	140[40]	105.3 ± 2.4	···	√	√	√	√

[a]Measured by ASTM 3767 Standard Practice for Rubber-Measurement Dimensions (thickness); measurement instrument: micrometer.
[b]Thickness of membranes after mechanical deformation; measurement instrument: scanning electron microscope (SEM) measurements on membrane cross sections.
[c]CGSB: Canadian General Standards Board; follows standards such as ISO 11193-1 regulating dimensions and physical parameters (mechanical strength, hole detection, etc).
[d]ASTM D6319: covers glove manufacturing and quality (dimensions, thickness, mechanical strength, etc.).
[e]ASTM F739: standard test for the permeation of liquids and gases through glove material; continuous contact of the glove material with the tested substance.
[f]ASTM F1671: standard test for resistance of glove material against the penetration by blood-borne pathogens.
[g]ASTM D6978: standard test for resistance of glove material against chemotherapeutic agents.
[h]ASTM D3578: covers rubber glove physical characteristics and quality (physical dimensions, tensile strength, and ultimate elongation).
[i]EN 420:2003: general requirements for glove material including size, dimensions, pH, and composition.
[j]FDA 21: general glove physical examination.
[k]FDA 510(k): general glove physical examination.

mechanical strength, and hole detection). For comparative purposes, the non-standardized nitrile gloves Sterling SG® and Aquasoft® were also selected because they are widely used in hospital and clinical work. For comparative purposes also, one well-characterized and standard-compliant latex membrane was also selected. Each one of the polymer membranes was carefully measured and characterized by scanning electron microscopy (SEM, for thickness and surface uniformity, see Sec. II G) prior to each experiment (Table I). In Table I, these values are compared with the thicknesses reported by the fabricant of each glove type; these measurements usually being performed by means of a micrometer. A micrometer provides an average measurement over a large surface (several mm^2, if not cm^2), whereas SEM measurements are performed at a comparatively very high magnification. Therefore, the lower thicknesses reported for the SEM measurements performed in the present study, compared with the thicknesses reported by the fabricant based on micrometer measurements, were expected.

When gloves are worn, hand and finger flexions stretch the polymer membranes. To simulate wear for a period of one hour, the membranes were mechanically deformed by a protocol adapted from the literature prior to mounting them in the diffusion cell.[23,41] Briefly, 9 × 4 cm^2 pieces were fixed in a vice clamp and stretched up to 50% deformation in one direction (x-direction) at a frequency of once per 5 min for 1 h. The same procedure was repeated in the y-direction.

G. Polymer membrane characterization

The thickness of the polymer membranes and the effect of mechanical stretching on the membrane surface were analyzed by SEM (FEI Quanta 250 SEM, Thermo Fisher, Oregon, USA). In addition, the membrane elemental and chemical compositions were analyzed by energy-dispersive x-ray spectroscopy (EDS, EDAX detector, Ametek USA) and ATR-FTIR (outer and inner surfaces), respectively. For ATR-FTIR, an Agilent Cary 660 system (Agilent Technologies, USA), equipped with a deuterated L-alanine-doped triglycine sulfate detector and a Ge-coated KBr beam splitter, was used. In addition to the polymer membranes, Au NPs were also characterized (see Sec. II B). The infrared absorption spectra from pure DFO and pure HS-PEG-COOH were also acquired as controls. The exact methodology is detailed in the supplementary material, Sec. S6.

H. Permeation data acquisition with the diffusion cell developed for operation in PET

A diffusion cell adapted to a small-animal PET system was specifically developed for the present study. The device is made of a DC and an AC of equal volumes [4.71 ml; 20 mm diameter, 15 mm height; Fig. 1(c)] and separated by a test membrane clamped inside of a cassette (Fig. 1). The two compartments are centered in the field of view (FOV) of the PET system described in Sec. II D. This diffusion cell was optimized based on a measurement test diffusion device also adapted to PET imaging, specifically developed for allowing topical measurement tests of contaminants across biological membranes (e.g., the skin).[30] The optimized version described here is a technology that is specifically developed for the standard measurement of molecule and nanoparticle kinetics across membranes immersed in fluids;[9] such standard measurements, widely used in the field of protective clothing, are not possible without a careful control over the fluid volume contained in both chambers (not possible using a topical diffusion study such as described in Ref. 30).

Permeation tests were run according to the ASTM standard F739 guidelines.[9] The membranes were fixed in the cassette. The US-AuNPs–^{89}Zr suspension containing 5.5 ml of 40.8 ± 2.3 μM US-AuNPs labeled with ~5MBq of ^{89}Zr (Au: Zr = 1:1.8× 10^{-5}) was placed in the DC (suspended in 70% ethanol or PBS), whereas the AC was filled with either 70% ethanol or PBS (1× − pH 7). Before

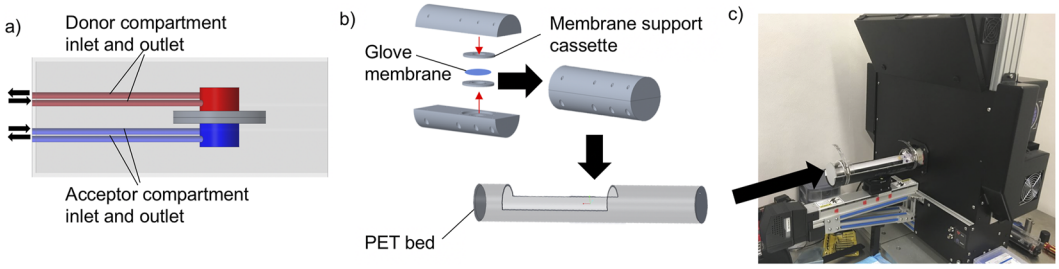

FIG. 1. Design and components of the PET diffusion cell for glove membrane permeation tests: (a) assembled PET diffusion cell; (b) schematic representation of the assembly and insertion in the PET holder; and (c) insertion of the diffusion cell in the PET system.

each diffusion experiment, the PET system was normalized by a ^{68}Ge rod. Image acquisition was performed in continuous for up to 42 h (procedure[30]). The images were then separated into 1 h frames with an axial thickness of 0.3 mm and a voxel size of 0.3 × 0.3 × 0.3 mm^3 (ordered subset expectation maximization reconstruction algorithm, OSEM, 4 subsets, 20 iterations). All permeation experiments were performed in triplicate.

At the end of each experiment, the cell was emptied and the membrane surface was dried on both sides using a tissue (Kimwipes Kimtech, Kimberly-Clark, USA). The activity remaining inside the membrane was then measured by gamma counting (in cpm) and then converted in MBq (correlation curves, supplementary material). The remaining DC and AC fluids as well as the polymer membranes were sampled and kept for post permeation analysis.

I. Permeation data analysis

In each reconstructed time frame of the PET images, the axial layer corresponding to the middle of the DC and AC was selected for signal integration (as described in Ref. 30). Regions of interest (ROI) were drawn over volumes of the DC and of the AC (cylinders of 14.5 mm in diameter and 9 mm in height total volume of 1.5 ml, 59 515 voxels each). The intensity (in cps) was integrated over each ROI and then corrected for decay and plotted (in counts per hour) as a function of time for each one of the compartments.

The background in each experiment was taken as the lowest detected activity in the AC in the first hours of the experiment and reported to a period of 1 h. The background was subtracted from both AC and DC hourly count values. Finally, the data were normalized to the total activity detected in the DC in the first minutes of each experiment. The activity data were converted in values of concentration of AuNPs using the calibration curves (see Sec. II D) and plotted as a function of time for each one of the compartments (DC and AC). In brief, the activity contained in 5.5 ml of US-AuNPs–^{89}Zr disposed in the DC at the beginning of the experiment represented a concentration of 40.8 ± 2.3 μM (Au) and a total amount of Au of 0.192 μmol. An activity of ~5MBq in ^{89}Zr was used in each experiment for a Au:Zr ratio of ~1:1.8× 10^{-5}.

J. Permeation profile data analysis and parameter calculations

The AC permeation profiles were used to evaluate the particle lag time to permeation (τ), the diffusion coefficient (D), the average influx at pseudo-steady-state ($\bar{J}_{pss}$), and the average total influx ($\bar{J}_T$) of the gold NPs across each type of membrane and under different fluid conditions. The theory and the mathematical equations are described in detail in the supplementary material, Sec. S7.

Overall, US-AuNPs–^{89}Zr (A_T) can be divided into three "pools": one population in the DC (A_{DC}), one population in the AC (A_{AC}), and one population in the glove membrane (A_{glove}). The amount of US-AuNPs–^{89}Zr accumulating in the polymer membrane at each time point (i) was deduced using the following equations:

$$A_T = A_{DC} + A_{AC} + A_{glove}, \quad (1)$$

$$A_{glove} = A_T - A_{DC} - A_{AC}. \quad (2)$$

K. Post permeation analysis

Stability of US-AuNPs–^{89}Zr: after each permeation experiment, the stability of ^{89}Zr chelation in US-AuNPs was verified to demonstrate the absence of free ^{89}Zr ions in the measured solutions (supplementary material, Sec. S3).

Microwave Plasma-Atomic Emission Spectrometer (MP-AES): the gold concentration in the DC and the AC was measured at the end of each experiment. The final solutions were digested and measured by MP-AES (supplementary material, Sec. S8).

Fourier Transform Infrared Spectroscopy (FTIR): at the end of the permeation experiments, the membranes were analyzed by ATR-FTIR to detect the presence of US-AuNPs in their structure (as in Sec. II G).

III. RESULTS

A. Nanoparticles synthesis and characterizations

The US-AuNPs synthesized for this study had a mean average core size of 3.3 ± 0.1 nm according to TEM data [Figs. 2(a) and 2(b)], while the hydrodynamic diameter was found to be 18.2 nm in water, 13.5 nm in PBS 1×, and 28.2 nm in 70% ethanol [Fig. 2(c)]. These size and morphological properties agree well with the general characteristics of USNPs used in nanomedicine and that represent a high risk of diffusion into the skin.[31–35] Interestingly, the DLS results indicate that PEG polymer chains on the US-AuNPs tend to contract in PBS 1× (high salt content), while they tend to relax in alcoholic

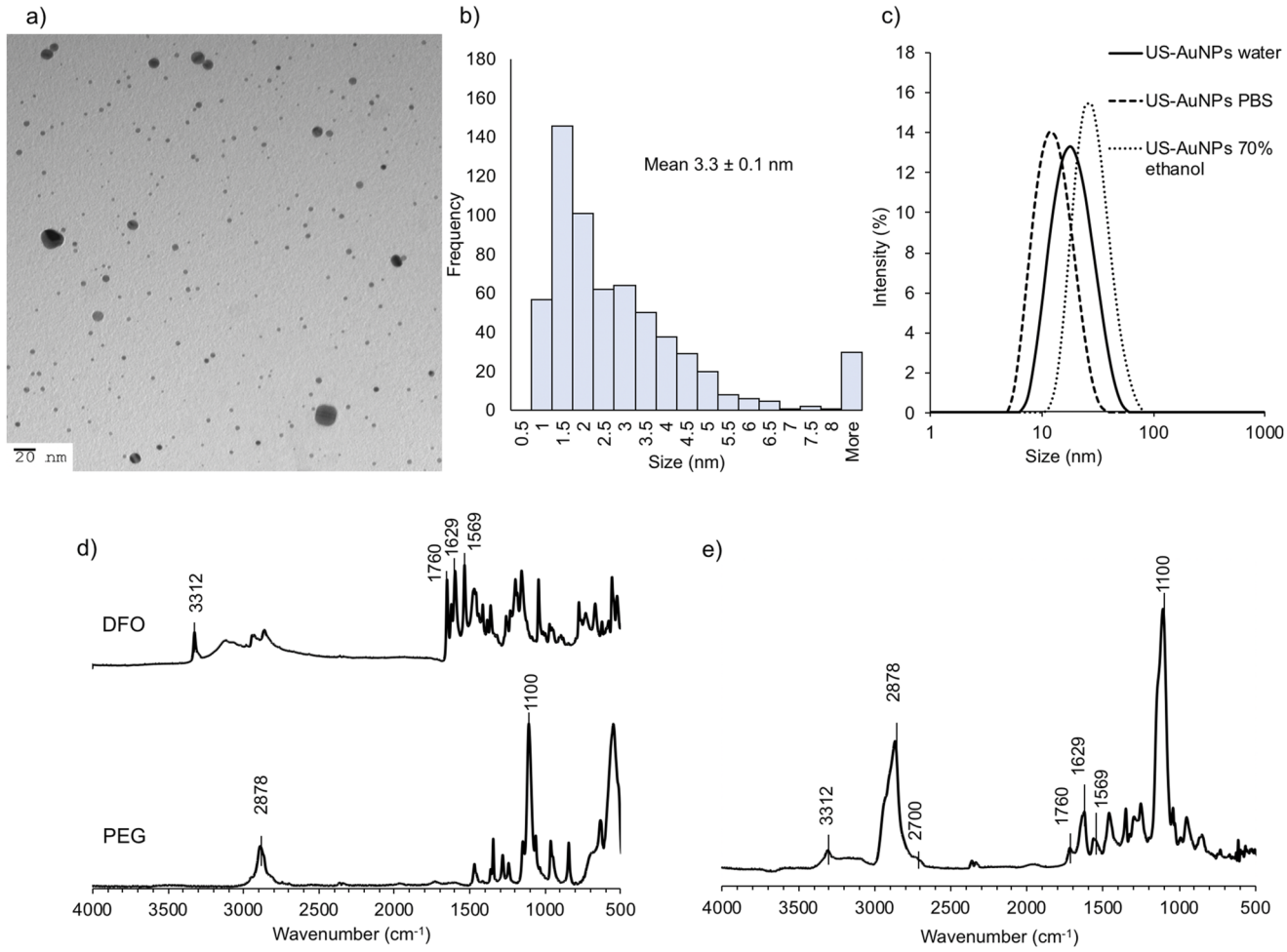

FIG. 2. Physico-chemical analysis of US-AuNPs. (a) TEM image of US-AuNPs. (b) Corresponding size distribution. (c) Intensity weighted DLS profiles for US-AuNPs in nanopure water (PDI:0.186), PBS 1× (PDI: 0.161), and 70% ethanol (PDI: 0.167). (d) and (e) FTIR spectra of HS-PEG-COOH, DFO, and US-AuNPs, showing the presence of PEG-COOH and DFO at their surface.

media (70% ethanol).[42–44] Overall, the sharpness of the DLS peaks at dimensions below 50 nm, and the absence of any other contribution at higher hydrodynamic diameters, confirm that the colloid suspension is robust, is not agglomerated, and conforms well to the requirements of this measurement study.

The FTIR spectrum of US-AuNPs [Fig. 2(e)] reveals bands typical of the PEG-COOH molecules used as a stabilizing ligand: C–H stretching at 2878 cm^{-1} as well as the characteristic aliphatic ether C–O–C stretching at 1100 cm^{-1}.[45] The band typical of the Au–S–CH vibration (2700 cm^{-1}) also confirm the bonding of PEG at the NP surface. Bands typical of the DFO molecules used for complexation of the ^{89}Zr ions at the surface of US-AuNPs are also revealed: hydroxamate amide peak I and II at 1629 and 1569 cm^{-1}, respectively, and the NH stretching peak at 3312 cm^{-1} as well as the DFO C–N stretching and N–H bending at 1259 cm^{-1}.

B. Characterization of polymer membranes

SEM analysis was performed on polymeric membranes before and after mechanical deformation in order to reveal the potential presence of pores that could indicate the possibility of NP permeation.[46]

Latex is generally more elastic than nitrile.[46,47] The latex membranes selected in this study present irregular striae [Figs. 3(a) and 3(b), red arrowheads], which after deformation appear larger [Figs. 3(c) and 3(d), red arrowheads]. This is an observation often reported in the literature.[46] Surfaces of the three nitrile membranes do not reveal the same patterns. However, holes and striae were present in each one of the membranes. N1 nitrile showed evidences of round-shaped holes [Figs. 3(e) and 3(f)], whereas flatter surfaces showing cracks were evidenced on the mechanically deformed samples [Figs. 3(g) and 3(h)]. N2 nitrile membranes showed similar evidences of holes, although more irregularly distributed [Figs. 3(i)

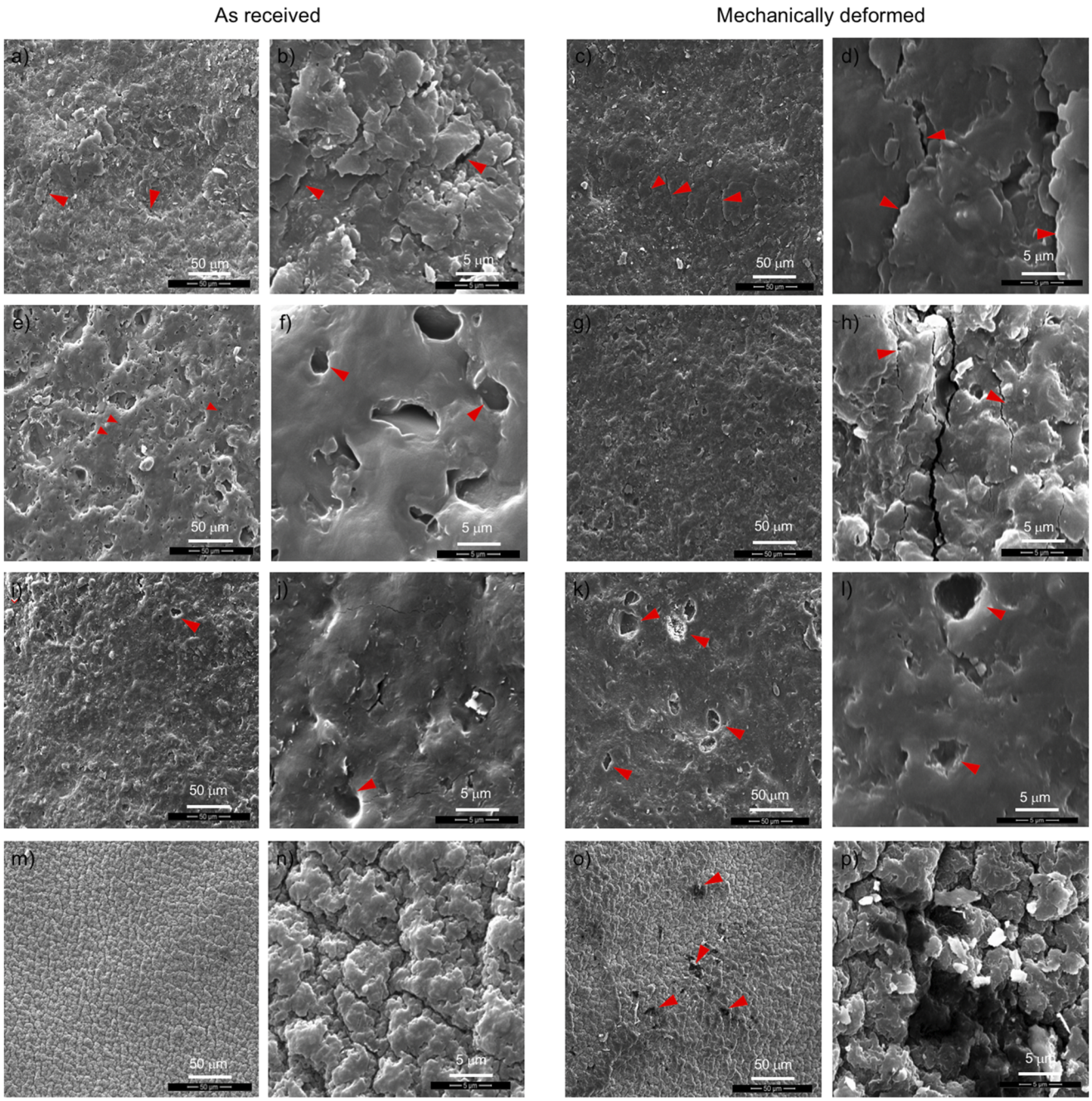

FIG. 3. SEM images of membranes before and after mechanical deformation. Latex (L1) (a) and (b) before and (c) and (d) after deformation. Nitrile N1 (e) and (f) before and (g) and (h) after deformation. Nitrile N2 (i) and (j) before and (k) and (l) after deformation. Nitrile N3 (m) and (n) before and (o) and (p) after deformation. Magnifications: ×5k and × 50k. Red arrows point to significant signatures identified in the study (described in the text).

and 3(j)]. After mechanical deformation, large defects appear and holes appear widened [Figs. 3(k) and 3(l)]. This behavior is characteristic of nitrile membranes submitted to mechanical solicitation.[46] Finally, the texture of N3 nitrile membranes appeared more uniformly patterned [Figs. 3(m) and 3(n)]. Upon stretching, these revealed large pores [Figs. 3(o) and 3(p)]. Overall, SEM analysis on mechanically deformed polymer membranes revealed significant morphological changes that help the interpretation of particle

permeation profiles revealed in the PET diffusion cell study (later in the text). Overall, minimal changes were noted for the latex membranes compared with those observed in the nitrile membranes.

EDS analysis of the membranes (Sec. S9, Table S1) revealed $CaCO_3$ and TiO_2 used for coloration of the glove membranes.[48] Latex membranes showed a quite strong atomic concentration of Ca (2.7%), whereas N1 contained Ca, Ti, and Zn (0.4%, 0.4%, and 0.1%,

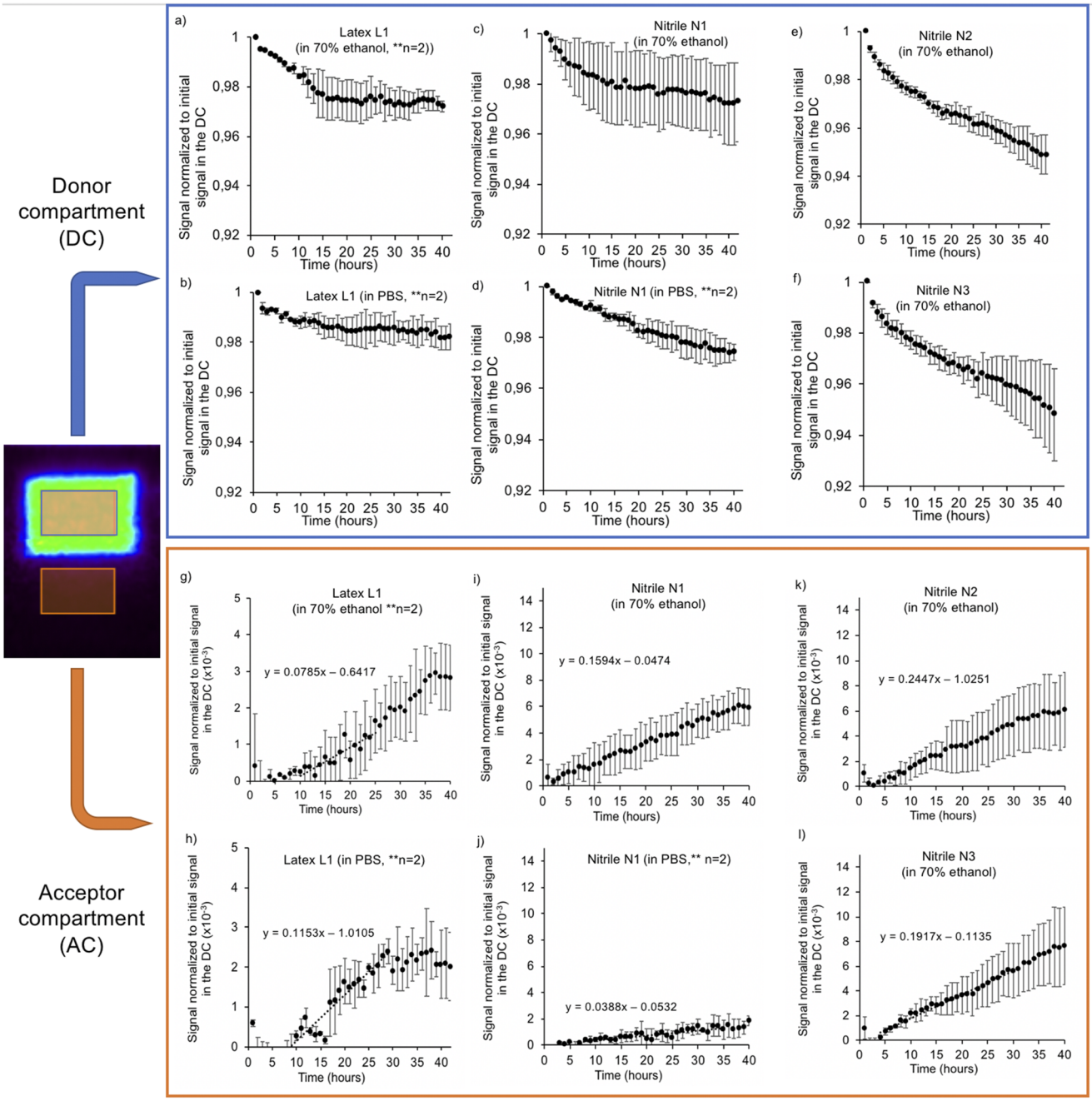

FIG. 4. Permeation profiles of US-AuNPs–^{89}Zr in 70% ethanol and in PBS 1×, acquired by PET imaging in the DC and the AC. At the left, a cross section of a PET image typically used for extraction of the signal in the volumes corresponding to the DC and the AC. Equations on the graphs correspond to the linear projections of the pseudo-steady-state regime. All results are for mechanically deformed membranes.

respectively). Zn was present in each nitrile membrane but not in latex. Zn is attributed to the crosslinking mechanism used in the production of nitrile. N2 membranes showed the presence of Cl, Ca, Ti, and Zn (0.6%, 0.4%, 0.2%, and 0.1%, respectively). Finally, a lower presence of metals was found in N3 membranes with Ca and Zn at 0.3% and 0.2%, respectively.

C. Sensitivity of the PET system to the detection of NPs

The cross correlation curve established between gamma counting, PET scanning, elemental analysis (MP-AES), and UV–visible absorption spectrometry, demonstrated the possibility to detect with both PET and gamma counter, a concentration of US-AuNPs down to 0.002 μM of gold (supplementary material, Fig. S3). In fact, for the radioactive US-AuNP solutions used in the study (Au:^{89}Zr ratio kept at 1:1.8 × 10^{-5}), LODs of ~20, <0.002, and ~0.002 μM were found for UV–visible, gamma counting, and PET scanning, respectively.

D. Nanoparticle permeation measurements with PET imaging

Permeation experiments were performed both in 70% ethanol and in PBS 1×, two media that are widely used in clinical practice and in biomedical laboratories. Each one of the permeation graphs revealed the diffusion of the US-AuNPs–^{89}Zr out of the DC [Figs. 4(a)–4(f), gradual decrease] and into the AC [Figs. 4(g)–4(i), gradual increase]. For all latex and nitrile membranes tested and under each fluid condition, the decrease in AuNP concentration in the DC did not exceed 6%–7%, justifying the use of the pseudo-infinite dose model (supplementary material, Sec. S7). The data plotted in Fig. 4 confirm that diffusion cell measurements performed in PET allow for the real-time detection of AC permeation and this in the nanomolar concentration range. Latex L1 and nitrile N1, the two types of membranes that comply with the highest number of standards for glove production (Table I), are also associated with the lowest DC losses (not more than 3.6%). The comparison between tests performed in 70% ethanol and in PBS reveals a higher permeation of AuNPs in 70% ethanol compared with PBS 1×.

The varying magnitude of the error bars agrees with the heterogeneous presence of porosities detected in the membranes (SEM results, Fig. 3). This variability is not induced by the PET measurement technology but rather by the heterogeneity of membrane quality between each one of the samples.[49] These differences are exacerbated by the mechanical deformation cycle applied to the membranes. For the latex membranes [Figs. 4(a), 4(b), 4(g), and 4(h)], the increase in US-AuNP concentration in the AC was very moderate in the first 15 h, followed by a strong increase, and then by a relative plateau after 30 h. Similar values of US-AuNP

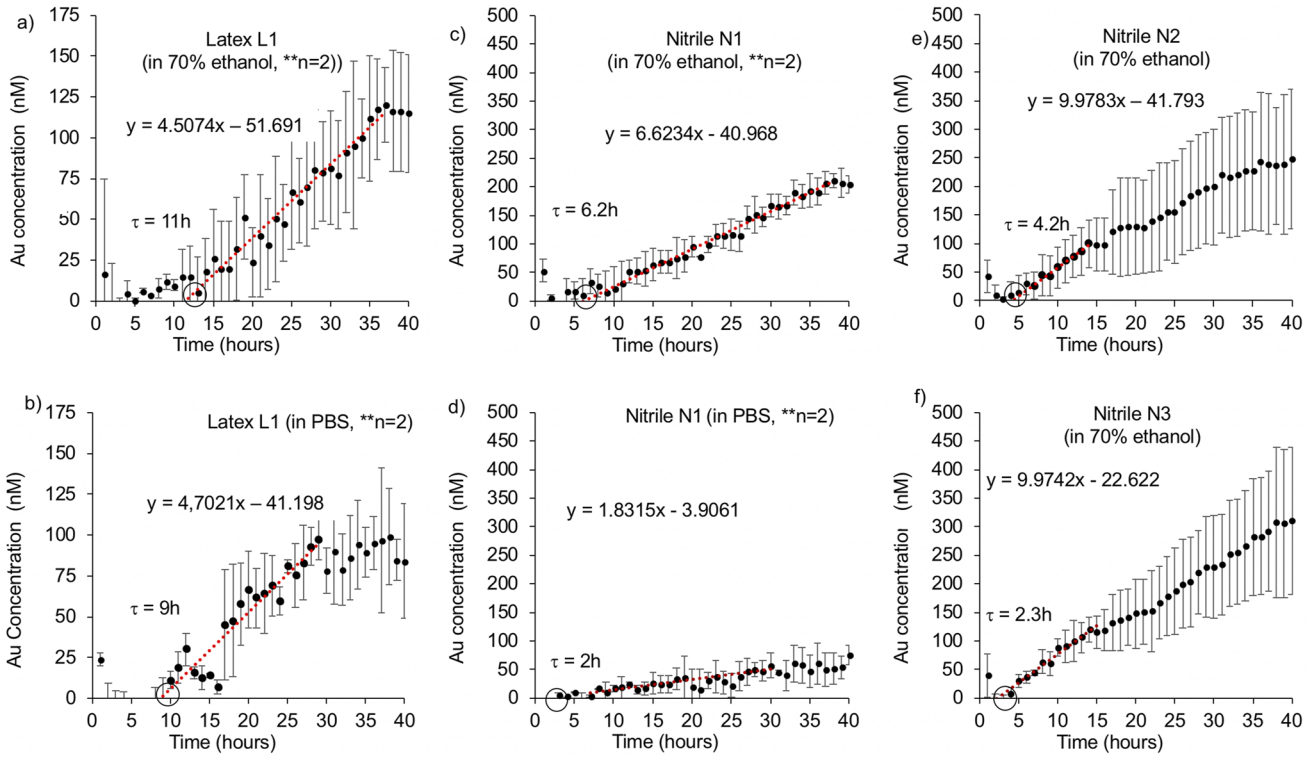

FIG. 5. Permeation of US-AuNPs–^{89}Zr through polymeric membranes in 70% ethanol and in PBS; Y-axis: cps units were converted in Au molar concentration values. Circles: lag time to start of permeation. Equations on the graphs correspond to the linear projections of the pseudo-steady-state regime. All results are for mechanically deformed membranes.

TABLE II. Summary of permeation parameters measured with latex and nitrile gloves exposed to 70% ethanol and phosphate buffer saline solution (PBS 1×) (calculation of uncertainties described in the supplementary material, Sec. S10).

	Membrane type					
	Tested in 70% ethanol				Tested in PBS 1×	
	Latex L1	Nitrile N1	Nitrile N2	Nitrile N3	Latex L1	Nitrile N1
	Constants					
Thickness (x) (cm)	0.0105 ± 0.0002	0.0052 ± 0.0003	0.0053 ± 0.0003	0.0043 ± 0.0003	0.0105 ± 0.0002	0.0052 ± 0.0003
	Data extracted from the AC					
Lag time to permeation (τ) (h)	12 ± 2	6.2 ± 0.8	4.2 ± 0.8	2.3 ± 0.7	9 ± 2	2 ± 1
Diffusion coefficient (D) ($x^2/6\tau_{ss}$) (cm^2 h^{-1})	$1.6 \pm 0.2 \times 10^{-6}$	$7.3 \pm 0.9 \times 10^{-7}$	$1.1 \pm 0.2 \times 10^{-6}$	$1.4 \pm 0.5 \times 10^{-6}$	$2.1 \pm 0.6 \times 10^{-6}$	$2 \pm 2 \times 10^{-6}$
Average influx at pseudo-steady-state ($\bar{J}_{pss}$) (nmol cm^{-2} h^{-1})	0.0079 ± 0.0004	0.0116 ± 0.0003	0.017 ± 0.001	0.017 ± 0.001	0.0082 ± 0.0007	0.0032 ± 0.0002
Average total influx ($\bar{J}_T$) (nmol cm^{-2} h^{-1})	0.005 ± 0.002	0.0089 ± 0.0006	0.011 ± 0.005	0.014 ± 0.006	0.004 ± 0.002	0.0033 ± 0.0007
Total flux of Au NPs through the experiment (40 h; in nmol Au)	0.6 ± 0.2	1.12 ± 0.08	1.4 ± 0.7	1.7 ± 0.7	0.5 ± 0.2	0.41 ± 0.09

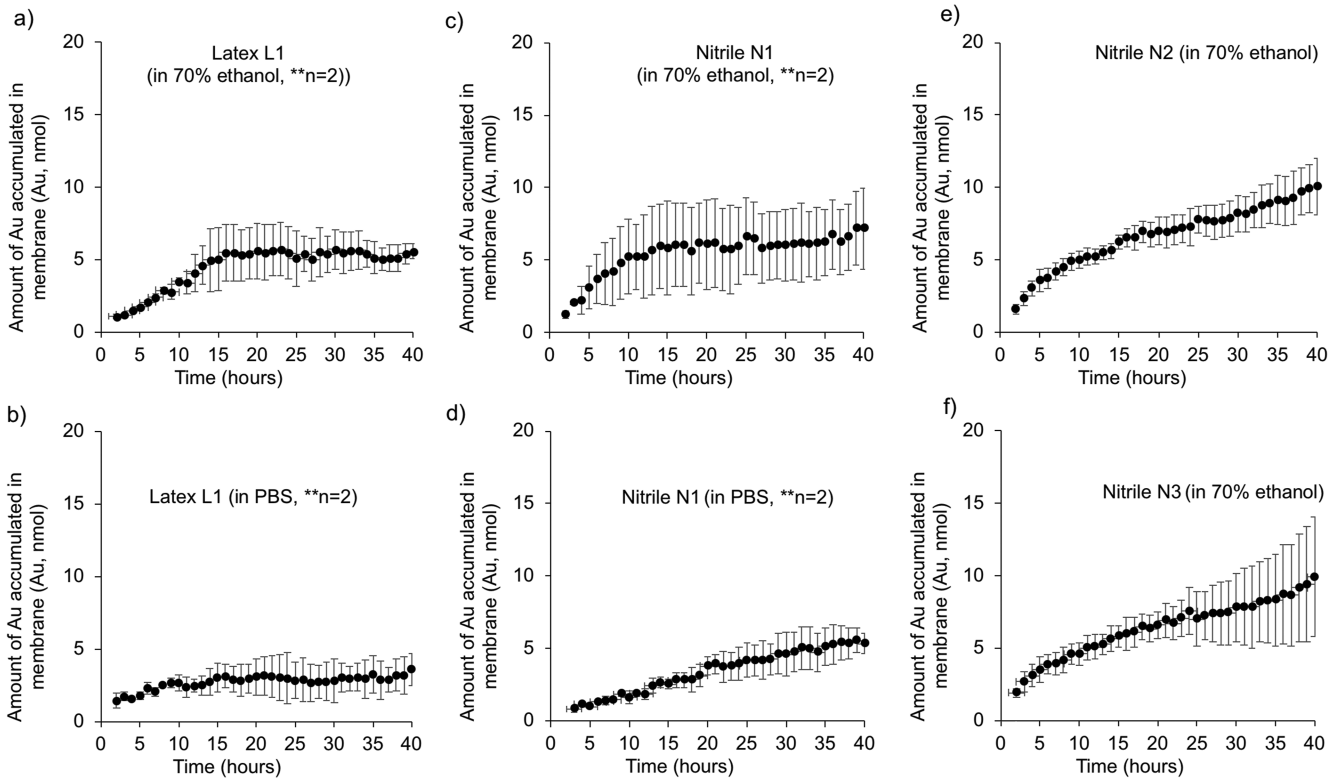

FIG. 6. Accumulation of US-AuNPs–^{89}Zr in polymer membranes obtained by subtracting the signal loss in the DC from the signal accumulated in the AC.

concentration in the AC were found after exposure of the latex membrane to 70% ethanol and to PBS 1×.

For the nitrile membranes, the increase in US-AuNP concentration in the AC was very constant, almost linear for each type of membrane and under each condition [Figs. 4(c)–4(f) and 4(i)–4(l)]. The three nitrile membranes measured in 70% ethanol revealed very similar AC permeation profiles: a linear profile reaching at 40 h a maximum of 0.6%–1.2% of the total initial dose injected in the DC as well as error bars all in the same magnitude range. However, the large error bars noted for the samples N2 and N3 exposed to ethanol point to possibly larger defects in these membranes, which cause higher variability over time. The difference in signal between the samples is further exacerbated by the application of the decay factor for ^{89}Zr for all results (this factor increases for the longer counting times). Finally, exposure of nitrile to PBS seems to impede the permeation of US-AuNPs compared with the same test performed in 70% ethanol [Figs. 4(i) and 4(j)].

At the end of each experiment (40–42 h), US-AuNPs–^{89}Zr were collected in the DC, and a chelation stability assay was performed to confirm the strength of ^{89}Zr chelation to DFO (supplementary material, Sec. S3, and Fig. S2). By using the correlation curves (supplementary material, Sec. S4, and Fig. S3), the permeation graphs were converted from normalized intensity data to nanomoles of Au leaving the DC and entering the AC (Fig. 5). The circles indicate the lag time to the start of permeation (τ) determined by the interception of the pseudo-steady-state line (red dashed) with the x-axis. Overall, the concentration of AuNPs detected in the AC never exceeded 500 nM even after 40 h of permeation and for an initial concentration of 40.8 μM injected in the DC. Therefore, equilibrium conditions between the DC and the AC, which would be revealed by the presence of a linear section on the curve, were not reached during the experiment.

Interestingly, a slight activity is often detected in the first hour of each test, which is attributed to the very small fraction of free ^{89}Zr (unchelated) passing through the membrane rapidly. After 1 h, it possibly reacts with the membrane or with the surfaces of the cell since invariably the signal goes down to close to 0 before increasing again after a certain lag time (τ) characteristic of each membrane. For latex membranes, very long lag times are revealed (12 ± 2 and 9 ± 2 h for 70% ethanol and PBS, respectively). For N1, the lag times were 6.2 ± 0.8 and 2 ± 1 h in 70% ethanol and in PBS, respectively. Shorter lag times were obtained for N2 and N3 membranes tested in 70% ethanol (4.2 ± 0.8 and 2.3 ± 0.7 h, respectively). This variability in the lag times observed between each one of the membranes has a strong impact on the diffusion coefficients (Table II).

Kinetic data were extracted from the graphs of Fig. 5. As revealed in Table II, the diffusion coefficients of AuNPs across latex and polymer membranes were all found in the range between 7.3×10^{-7} (for N1 in 70% ethanol) and 2.1×10^{-6} cm^2 h^{-1} (for L1 in PBS ×1). These are typical values expected for macromolecules or nanostructures diffusing into well-structured and compact material membranes such as latex and nitrile.[46] As for the total influx of US-AuNPs in the membranes, in 70% ethanol, the figures were twice higher for the nitrile membranes (all types) compared with the latex ones. In PBS, however, a total influx number of similar magnitude was obtained in latex and in nitrile (N1). Finally, the total flux of US-AuNPs passing through the membrane after 40–42 h of permeation is all included between 0.41 and 1.4 nmol of Au.

For an initial DC volume of 5.5 ml at 40.8 μM of AuNPs, latex membranes soaked in 70% ethanol allowed for a total permeation of 0.6 ± 0.2 nmol Au, whereas in PBS, this permeation was slightly lower (0.5 ± 0.2 nmol Au). Nitrile N1 membranes permeated more NPs in 70% ethanol (1.12 ± 0.08 nmol Au) compared with PBS (0.41 ± 0.09 nmol Au). Among all nitrile membranes tested in 70% ethanol, relatively similar permeation values were revealed at 40 h (1.12 ± 0.08, 1.4 ± 0.7, and 1.7 ± 0.7 nmol Au for N1, N2, and N3, respectively). These values agree with the higher degree of quality compliance reported for membranes L1 and N1 (Table I). The nanomolar detection sensitivity achieved by PET is of the same order of that typical of ICP-MS, the most sensitive technique for elemental analysis. However, PET measurement is performed in real-time and without sampling in the AC, which is a strong advantage of the technology.

From Figs. 4 and 5 and Table II, it is clear that only a fraction of US-AuNPs–^{89}Zr exiting the DC does reach the AC. This difference between the values reveals the strong retention of NPs inside the glove membranes. For each membrane, this amount was quantified by subtracting the amount of AuNPs exiting the DC by the amount entering in the AC (Fig. 6). A steady accumulation of AuNPs

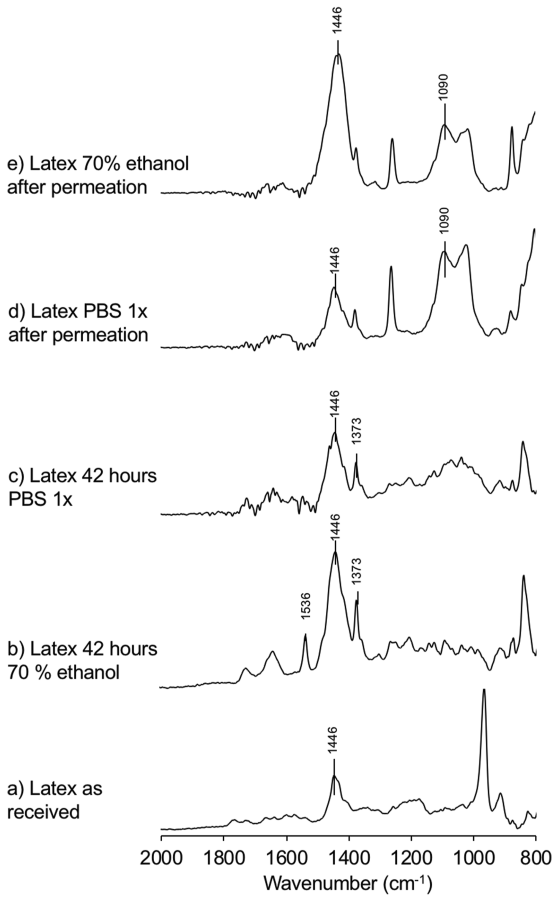

FIG. 7. FTIR spectra of the inner side of latex gloves (from 2000 to 800 cm^{-1}) after different treatments listed from (a)–(e).

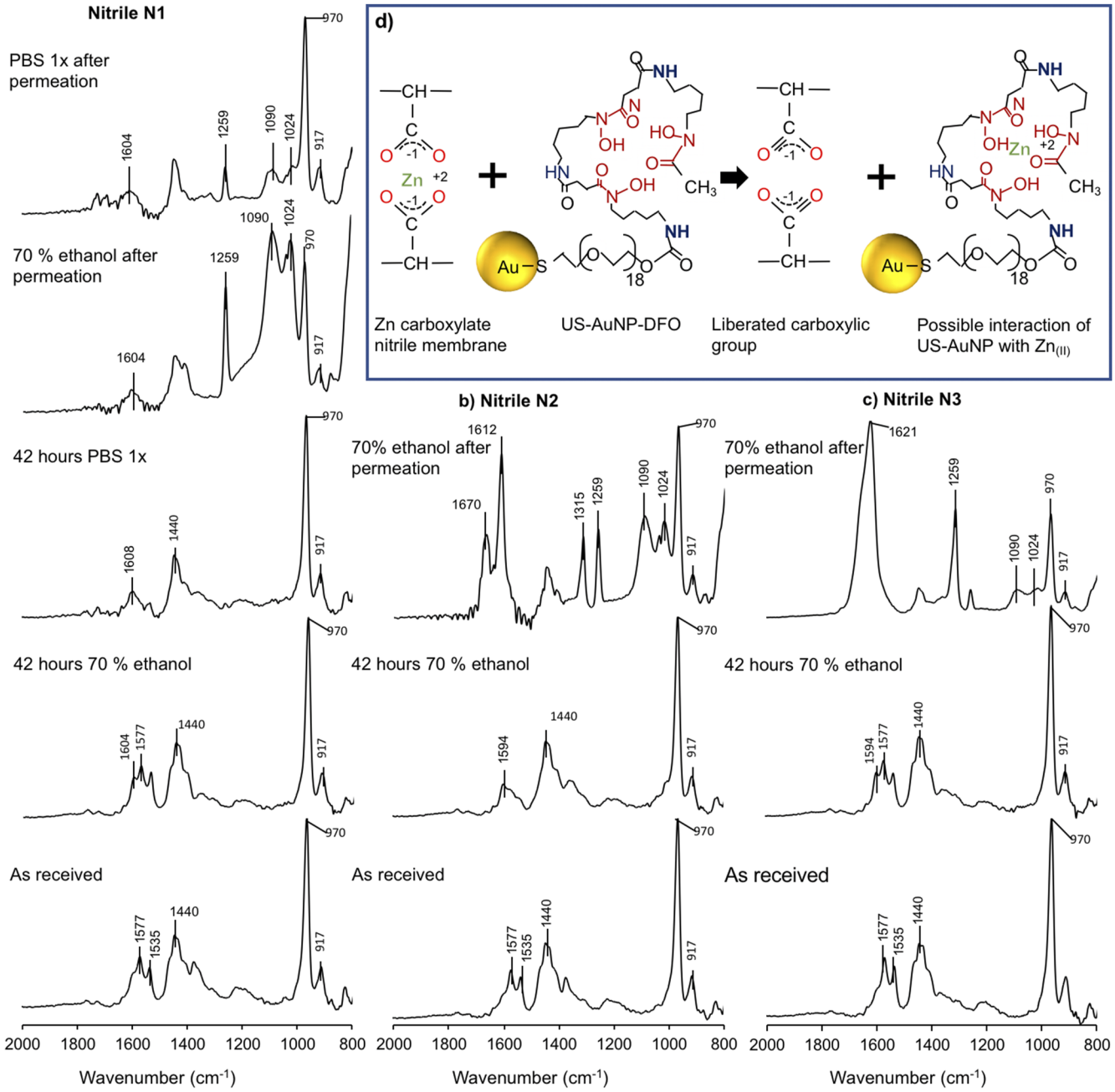

FIG. 8. FTIR analysis of nitrile membranes (a)–(c); as received after immersion in PBS 1× and 70% ethanol as well as after US-AuNPs permeation. (d) Proposed scheme for the interaction of $Zn_{(II)}$ atoms contained in the nitrile membranes with the DFO group bound to the surface of US-AuNPs.

in polymer membranes was thus revealed. The relatively large error bars are not due to the PET measurement technique but rather to the varying state of porosity observed across each one of the membranes tested. In fact, higher porosity in the membranes could be associated with a higher diffusion of NPs in the AC and to a lower retention in the membranes. This heterogeneity in the membranes, the limited amount of AuNPs reaching the AC and the subtraction operation (DC − AC) as well as the application of the decay factor for ^{89}Zr for all results (this factor increases for the longer counting times) lead to relatively large error bars, in particular, for Figs. 5(e) and 5(f). Latex

submitted to PBS conditions indicated a relatively constant amount of AuNPs in the membranes in the period 10–40 h.

Finally, at the end of each test, the membranes were collected, thoroughly washed, and the radioactivity was measured by a gamma counter. The values were converted in units of Au nanomoles (nmol) using the correlation curves (supplementary material, Fig. S4). For the latex membranes, total accumulations of 5.0 ± 2.0 nmol and 3.2 ± 1.8 were revealed for 70% ethanol and PBS conditions, respectively, whereas figures of 3.9 ± 1.6 nmol and 4.3 ± 1.5 were found for N1 nitrile membranes. For N2 and N3 tested in 70% ethanol, values of 6.8 ± 2.7 and 5.8 ± 2.3 nmol were found. Overall, these data acquired by gamma counting separately from PET measurements correlated very well with the total accumulation of AuNPs indicated by the subtraction of the PET signal integrated from the AC volume from the PET signal integrated from the DC volume (Fig. 6).

E. Physico-chemical characterization of polymer membranes before and after nanoparticle permeation

At the end of the PET measurement tests, the membranes were collected and their physico-chemical characteristics were studied by FTIR. The FTIR spectra of membranes submitted to the permeation process and after immersion in the two fluids (controls) are shown in Figs. 7 and 8. The chemical structures of latex and nitrile as well as the complete spectra are illustrated in the supplementary material (Sec. S11, Figs. S5–S7). Latex membranes showed evidences of degradation after immersion in 70% ethanol. This effect is indicated by specific chemical bands (different FTIR spectra for the inner and the outer surfaces, Fig. S5). Upon immersion in PBS 1 X, these effects are less pronounced. After permeation of US-AuNPs, the characteristics bands of the PEG-COOH molecules used as a stabilizer on the NPs are revealed, such as the characteristic aliphatic ether C–O–C stretching at 1100 cm^{-1} (Figs. 2 and 7).[45] Moreover, bands related to DFO are also noted. These results confirm the accumulation and the permeation of US-AuNPs through the latex membranes.

Nitrile membranes are usually formed of a polymer backbone consisting of acrylonitrile, butadiene, and carboxylic butadiene groups present in varying ratios (Fig. S7). The polymer backbones are linked either by ionic crosslinking (involving $Zn_{(II)}$), sulfur bridges, or both. In this study, Zn was detected in all nitrile membranes (Table S1, EDX results). In these membranes [Figs. 8(a)–8(c), as received spectra], the asymmetric and symmetric $Zn_{(II)}$ carboxylate stretching vibrations at 1577 and 1535 cm^{-1} are indicators of the ionic interaction between $Zn_{(II)}$ and the –COOH groups of the membranes.[50]

After 42 h of immersion in 70% ethanol, a clear peak at 1604 cm^{-1} was revealed for nitrile N1 and nitrile N3, corresponding to the formation of hydrogen bonds between the –OH group of ethanol and the butadiene Zn ionic carboxylate group [Figs. 8(a)–8(c), 42 h 70% ethanol]. With nitrile N2 in 70% ethanol and nitrile N1 in PBS 1×, the ionic carboxylate bond at 1577 cm^{-1} is shifted to about 1594 cm^{-1} [Fig. 8(a), 42 h PBS 1×], indicating a chemical degradation of these membranes.

After the permeation experiments, a strong band at ~1090–1100 cm^{-1} appeared in all materials and conditions, corresponding to the C–O–C stretching characteristic of PEG aliphatic ether bonds at the surface of the US-AuNPs (see also Fig. 2).[45]

In nitrile membranes, the $Zn_{(II)}$ carboxylate bands at 1577 and 1535 cm^{-1} disappeared [Figs. 8(a)–8(c), after permeation spectra]. In addition, new peaks at 1604 and 1621(intense) cm^{-1} appeared for nitrile N1 and nitrile N3 membranes, respectively. In N2 membranes, two intense peaks appeared at 1670 and 1612 cm^{-1}. These differences were ascribed to carbonyl stretching vibrations of the H-bonded –COOH group, which reveals the breakdown of the $Zn_{(II)}$ carboxylate bonds and the resulting liberation of hydrogen-bonded carboxylic groups. This mechanism is illustrated schematically in Fig. 8(d).

IV. DISCUSSION

US-AuNPs were radiolabeled with a positron emitter of a half-life matching the timescale of diffusion studies. Permeation profiles were acquired in two fluids (ethanol and PBS) with different types of polymer membrane representatives of gloves used by workers in skin care, drug delivery, and filtration technologies. Under each condition, two permeation curves were extracted from the PET images, one revealing the decrease in US-AuNPs from the DC and one reflecting the increase in the AC. Finally, the diffusion behavior of NPs across membranes was correlated with physico-chemical (FTIR, EDS) and microscopy (SEM) measurements.

PET has several advantages over the different measurement technologies commonly used with diffusion cells. First, the usual technologies are too low in sensitivity to allow a comprehensive measurement of kinetics data.[22,49,51] For instance, in 2016, Vinches *et al.* compared the permeation of two sizes of AuNPs [5 and 50 nm (TEM), 9.2 and 67.2 (DLS)] through nitrile membranes. Only one measurement was performed at the end of a 3 h permeation process, which confirmed the higher permeation of the smaller NPs. The concentration of Au was very close to the LOD of ICP-MS to guarantee reproducibility between the repeats.[51] Finally, in 2017 and in a similar type of study, Vinches *et al.* measured the decrease in 5 nm AuNPs in the DC solution after several hours. However, no permeation profiles were reported in this study, and the reported levels of variability among ICP-MS measurement repeats in the AC were in the order of 200%.[49]

The real-time high sensitivity measurements achieved by a diffusion cell operated in a PET equipment opens new possibilities in the field of membrane permeation measurements. The approach allows for the detection of lag times in a very precise manner. The lag time is a very important diffusion parameter, which depends on the thickness of the membrane and the surface area exposed to the permeating chemical as well as the experimental setup.[6] The accuracy of lag time determination depends on the sensitivity of the analytical technique employed: the more sensitive the analytical technique, the more accurate and precise the measurement.[6,9] If an imprecise or a poorly sensitive measurement technique is used, the exact moment at which contaminants reach the AC is simply missed. This cannot be the case with a technique as sensitive as PET. Finally, the technology allows for the precise measurement of influx rates and diffusion coefficients.

V. CONCLUSION

A diffusion cell adapted to the highly sensitive PET detection technology was used to measure the kinetic parameters of nanopar-

ticle diffusion across polymer membranes used to produce personal protective equipment (gloves). US-AuNPs were radiolabeled with a positron emitter of a half-life matching the time scale of the diffusion measurements. A selection of gloves among the most widely used by workers in the biomedical sector involved in NP production and manipulation were employed for the permeation tests. The permeation profiles were performed in real-time, and the diffusion process of NPs across polymers membranes was resolved in a very precise manner.

US-AuNPs were found to permeate faster through latex and nitrile membranes soaked in 70% ethanol compared with PBS. In general, the permeation process was stronger in nitrile membranes compared to latex; longer lag times to permeation were also found for the latex membranes. Unstandardized nitrile membranes showed the highest permeation to NPs and also the strongest accumulation of NPs. The kinetic parameters revealed by the measurement process were correlated with a physico-chemical analysis study of the polymers before and after the diffusion process, which confirmed the higher degradation of membranes soaked in 70% ethanol.

The results reported in this article are the first demonstration of the application of nuclear imaging to the measurement of a NP permeation process across polymer membranes used as personal protective equipment (PPE). The development of advanced permeation tests allowing the extraction of kinetic diffusion parameters for NPs and toxic molecules diffusing across polymer membranes is important in the field of pharmaceutics, cosmetics, and protective clothing. The technology and the experimental protocol reported in this article could be applied to the permeation process of several types of molecules and NPs that must be detected at high sensitivities, such as highly potent or toxic molecules (e.g., antineoplastic agents for chemotherapy, pesticides, etc.).

SUPPLEMENTARY MATERIAL

Complementary results are provided in the supplementary material.

ACKNOWLEDGMENTS

The authors would like to acknowledge the contribution of Dr. Pascale Chevallier from CR-CHU de Québec for FTIR analysis. This research project was financed by the Institut de Recherche Robert-Sauvé en Santé et Sécurité du Travail (IRSST: Grant No. 2015-0084, M.A.Fortin) and The Fonds de Recherche du Québec – Nature et Technologies (FRQNT; Ph.D. PBEE scholarship Grant No. 124274, M.M.Omar). PET studies were performed at the small animal imaging platform (CR-CHU de Québec – Université Laval).

AUTHOR DECLARATIONS

Conflict of Interest

The authors have no conflicts to disclose.

Author Contributions

Mahmoud Mohamed Omar: Conceptualization (equal); Data curation (equal); Formal analysis (equal); Investigation (equal); Methodology (equal); Writing – original draft (equal). **Mariia Kiseleva**: Formal analysis (equal); Investigation (equal); Methodology (equal). **Myriam Laprise-Pelletier**: Formal analysis (equal); Methodology (equal). **Amelie Auge**: Investigation (equal); Methodology (equal); Writing – review & editing (equal). **Ludovic Tuduri**: Conceptualization (equal); Validation (equal); Writing – review & editing (equal). **Marc-André Fortin**: Conceptualization (equal); Data curation (equal); Formal analysis (equal); Funding acquisition (equal); Investigation (equal); Methodology (equal); Project administration (equal); Resources (equal); Supervision (equal); Validation (equal); Writing – original draft (equal); Writing – review & editing (equal).

DATA AVAILABILITY

The data that support the findings of this study are available from the corresponding author upon reasonable request.

REFERENCES

[1] A. C. Anselmo and S. Mitragotri, Bioeng. Transl. Med. **4**(3), e10143 (2019).
[2] M. Wiszniewska and J. Walusiak-Skorupa, Curr. Allergy Asthma Rep. **15**(7), 43 (2015).
[3] F. Larese Filon, D. Bello, J. W. Cherrie, A. Sleeuwenhoek, S. Spaan, and D. H. Brouwer, Int. J. Hyg. Environ. Health **219**(6), 536–544 (2016).
[4] D. H. Brouwer, S. Spaan, M. Roff, A. Sleeuwenhoek, I. Tuinman, H. Goede, B. van Duuren-Stuurman, F. L. Filon, D. Bello, and J. W. Cherrie, Int. J. Hyg. Environ. Health **219**(6), 503–512 (2016).
[5] J. Cherrie, S. Semple, and D. Brouwer, in *Protective Gloves for Occupational Use*, 2nd ed. (CRC Press, 2004), pp. 229–253.
[6] G. A. Mellstrom, B. Carlsson, and A. Boman, in *Protective Gloves for Occupational Use* (CRC Press, Boca Raton, 2005), pp. 71–84.
[7] BS EN 374-2, British-Adopted European Standard, Brussels, Belgium, 2015, pp. 1–14.
[8] BS EN 455-1, British-Adopted European Standard, 2012, pp. 1–8.
[9] ASTM International ASTM F739, ASTM International, West Conshohocken, USA, 2012, pp. 1–10.
[10] ASTM International ASTM F1383, ASTM International, West Conshohocken, USA, 2012, pp. 1–13.
[11] ISO 6529, International Organization for Standardization, Genève, Switzerland, 2013, pp. 1–45.
[12] J. R. Heylings, in *Topical Drug Bioavailability, Bioequivalence, and Penetration*, edited by V. P. Shah, H. I. Maibach, and J. Jenner (Springer, NY, 2014), pp. 69–80.
[13] F. Larese Filon, M. Crosera, G. Adami, M. Bovenzi, F. Rossi, and G. Maina, Nanotoxicology **5**(4), 493–501 (2011).
[14] Evans Analytical Group, 2007, Vol. 2018.
[15] EN 374-1, in Part 1: Terminology and performance requirements, European Commission, Brussels, Belgium, 2016.
[16] EN 374-2, in Determination of resistance to penetration, European Commission, Brussels, Belgium, 2014.
[17] EN 374-3, in Determination of resistance to permeation by chemicals, European Commission, Brussels, Belgium, 2003.
[18] EN 374-4, in Determination of resistance to degradation by chemicals, European Commission, Brussels, Belgium, 2013.
[19] E. C. Dreaden, A. M. Alkilany, X. Huang, C. J. Murphy, and M. A. El-Sayed, Chem. Soc. Rev. **41**(7), 2740–2779 (2012).
[20] A. Z. Wilczewska, K. Niemirowicz, K. H. Markiewicz, and H. Car, Pharmacol. Rep. **64**(5), 1020–1037 (2012).
[21] A. Sharma, A. K. Goyal, and G. Rath, J. Drug Targeting **26**(8), 617–632 (2018).
[22] L. Golanski, A. Guiot, F. Rouillon, J. Pocachard, and F. Tardif, Hum. Exp. Toxicol. **28**(6-7), 353–359 (2009).
[23] L. Vinches, C. Peyrot, L. Lemarchand, N. Boutrigue, M. Zemzem, K. J. Wilkinson, S. Hallé, and N. Tufenkji, J. Phys.: Conf. Ser. **617**(1), 012030 (2015).

[24]J. Park, B. K. Kwak, Y. Kim, and J. Yi, J. Nanopart. Res. **13**(7), 3043–3049 (2011).
[25]A. C. Anselmo and S. Mitragotri, Bioeng. Transl. Med. **1**(1), 10–29 (2016).
[26]National Institute for Occupational Safety and Health Education and Information Division, 2018, Vol. 2018.
[27]National Institutes of Health Office of Research Services Division of Occupational Health and Safety, 2014, Vol. 2018.
[28]EU-OSHA, European Agency for Safety and Health at Work, Brussels, Belgium, 2009.
[29]Z12885-12, in Exposure Control Program for Engineered Nanomaterials in Occupational Settings, Canadian Center for Occupational Health and Safety, Ottawa, Canada, 2012.
[30]M. M. Omar, M. Laprise-Pelletier, P. Chevallier, L. Tuduri, and M.-A. Fortin, Bioconjugate Chem. **32**(4), 729–745 (2021).
[31]D. Cassano, S. Pocoví-Martínez, and V. Voliani, Bioconjugate Chem. **29**(1), 4–16 (2018).
[32]X. Jiang, B. Du, Y. Huang, and J. Zheng, Nano Today **21**, 106–125 (2018).
[33]B. H. Kim, M. J. Hackett, J. Park, and T. Hyeon, Chem. Mat. **26**(1), 59–71 (2014).
[34]M. Yu and J. Zheng, ACS Nano **9**(7), 6655–6674 (2015).
[35]K. Zarschler, L. Rocks, N. Licciardello, L. Boselli, E. Polo, K. P. Garcia, L. De Cola, H. Stephan, and K. A. Dawson, Nanomed.-Nanotechnol. Biol. Med. **12**(6), 1663–1701 (2016).
[36]M. Brust, M. Walker, D. Bethell, D. J. Schiffrin, and R. Whyman, J. Chem. Soc., Chem. Commun. **1994**(7), 801–802.
[37]Web-site: https://primed.com/resources/examination-glove-protection-standards-faq/ (consulted on 15 September 2022).
[38]Web-site: https://products.halyardhealth.com/infection-prevention/medical-exam-gloves/nitrile/sterling-sg-nitrile-exam-glove.html (consulted on 15 September 2022).
[39]Web-site: https://products.halyardhealth.com/infection-prevention/medical-exam-gloves/nitrile/aquasoft-nitrile-exam-glove.html (consulted on 15 September 2022).
[40]Web-site: https://www.ansell.com/ca/en/products/microflex-evolution-one-ev-2050 (consulted on 15 September 2022).
[41]P. Dolez, L. Vinches, K. Wilkinson, P. Plamondon, and T. Vu-Khanh, J. Phys.: Conf. Ser. **304**, 012066 (2011).
[42]M. H. Hussain, N. F. Abu Bakar, A. N. Mustapa, K.-F. Low, N. H. Othman, and F. Adam, Nanoscale Res. Lett. **15**(1), 140 (2020).
[43]M. J. Stevens and S. J. Plimpton, Eur. Phys. J. B **2**(3), 341–345 (1998).
[44]Testa Analytical Solutions, Testa Analytical Solutions, 2020.
[45]K. Shameli, M. B. Ahmad, S. D. Jazayeri, S. Sedaghat, P. Shabanzadeh, H. Jahangirian, M. Mahdavi, and Y. Abdollahi, Int. J. Mol. Sci. **13**(6), 6639–6650 (2012).
[46]P. Dolez, L. Vinches, G. Perron, T. Vu-Khanh, P. Plamondo, G. L'Espérance, K. Wilkinson, Y. Cloutier, C. Dion, and G. Truchon, "Development of a method of measuring nanoparticle penetration through protective glove materials under conditions simulating workplace use" (IRSST, Quebec, Canada, 2013); available at https://www.irsst.qc.ca/en/publications-tools/publication/i/100644/n/development-of-a-method-of-measuring-nanoparticle-penetration-through-protective-glove-materials-under-conditions-simulating-workplace-use-r-785.
[47]I. Furuta, S.-I. Kimura, and M. Iwama, *Polymer Handbook* (John Wiley & Sons, 2005), pp. V/1–V/7.
[48]H. P. Brown, Rubber Chem. Technol. **30**(5), 1347–1386 (1957).
[49]L. Vinches, M. Zemzem, S. Hallé, C. Peyrot, K. J. Wilkinson, and N. Tufenkji, J. Occup. Environ. Hyg. **14**(7), D95–D101 (2017).
[50]M. Létourneau, M. Tremblay, L. Faucher, D. Rojas, P. Chevallier, Y. Gossuin, J. Lagueux, and M.-A. Fortin, J. Phys. Chem. B **116**(44), 13228–13238 (2012).
[51]L. Vinches, M. Zemzem, S. Hallé, C. Peyrot, K. Wilkinson, and N. Tufenkji, Int. J. Theor. Appl. Nanotechnol. **4**, 9–16 (2016).